RSC Advances

ROYAL SOCIETY OF CHEMISTRY

www.rsc.org/advances

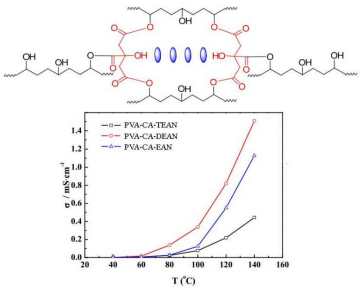

Anhydrous proton exchange membranes based on PVA and ILs can be applied at high temperature.

Anhydrous proton exchange membrane at elevated temperature: Effect of protic ionic liquids and crosslinker on proton conductivity

Yi Yang [a], Hejun Gao [b], Liqiang Zheng [a,*]

[a] Key Laboratory of Colloid and Interface Chemistry, Shandong University, Ministry of Education, Jinan 250100, China.

[b] Chemical Synthesis and Pollution Control Key Laboratory of Sichuan Province, China West Normal University, Nanchong 637000, China.

* Corresponding author: Liqiang Zheng, Prof. Ph.D.

Tel.: +86 531 88366062; Fax: +86 531 88564750.

E-mail address: lqzheng@sdu.edu.cn

Abstract

A series of novel anhydrous proton exchange membranes (poly (vinyl alcohol)-citric acid-ionic liquid (PVA-CA-IL)) were prepared using the low cost ionic liquids of ethylammonium nitrate (EAN), diethylammonium nitrate (DEAN), and triethylammonium nitrate (TEAN) as conductive fillers in PVA support membrane. The properties of the PVA-CA-IL membranes can be controlled by changing the molar ratio of the PVA, ILs and CA. The thermal stability of PVA-CA-IL membrane was measured by thermal gravity analysis (TGA) and differential scanning calorimetry (DSC), and the microstructure was investigated by scanning electron microscope (SEM) and Anton-paar SAX Sess mc2 system (SAXS). The effects of temperature, ILs and crossliker dosage on proton conductivity were also systematically investigated. The results showed that the PVA-CA-IL membranes had excellent performance. The proton conductivity of PVA-CA-EAN (mole ratio=1:0.05:0.4) could reach up to 7.8 $mS \cdot cm^{-1}$ at 140 $^{\circ}C$. The introduction of ionic liquid into PVA membrane constituted a new and efficient kind of anhydrous proton exchange membrane.

Keywords: Anhydrous proton exchange membrane; Ionic liquid; Poly (vinyl alcohol); High temperature

.

1. Introduction

With the development of industry and the inadequacy of energy resources, the sustainable energy of proton exchange membrane fuel cells (PEMFCs) receives a widespread interest by the researchers [1,2]. In the past years, PEMFCs has been widely applied in people's daily lives, such as aerospace, transportation, and as mobile power stations [3-5]. Proton exchange membrane (PEM) serves as the electrode separator in addition to its primary role as a continuous medium for conducting protons from anode to cathode [6-10]. The perfluoride-based membrane of Nafion® is the most common commercial PEMs, which shows an outstanding chemical stability and excellent proton conductivity [11,12]. However, the proton conductivity will decrease significantly at temperatures above 80 ˚C, which results from the evaporation of water in the membranes and thus limits proton mobility [13,14], and the membrane has very high cost and high fuel permeability [15,16]. These drawbacks of Nafion® hinder its future application. Therefore, the novel PEMFCs need to be developed earnestly.

In order to develop excellent PEMs, polymers such as polyimides, polybenzimidazole, poly(ether ether ketone) [17] and poly (vinyl alcohol) (PVA) have been mostly investigated [18-20]. Admittedly, PVA has attracted vast attention as excellent membrane materials because of the low cost, excellent fuel barrier, controllable physical properties and microstructures [21-23]. Won Rhim et al. [24] reported a novel crosslinked PVA membrane. The PEMs were prepared using poly(styrene sulfonic acid-co-maleic acid) (PSSA_MA) (PVA:PSSA_MA = 1:7) and Clay 15A, which achieved an excellent inhibition methanol performance (2.19×10^{-7}

$cm^2 \cdot s^{-1}$) and outstanding proton conductivity (0.023 $S \cdot cm^{-1}$). Gomes and Filho [25] successfully prepared a series of hybrid membranes using PVA, phosphotungstic acid and (diethylenetriamine)pentaacetic acid and found that the maximum conductivity can reach to 8.59×10^3 $S \cdot cm^{-1}$. Thanganathan and Nogami [26] synthesized a new class of hybrid nanocomposite membranes by sol-gel method, which contained PVA, phosphotungstic acid, 3-glycidyloxypropyltrimethoxysilane, 3-mercaptopropyltrimethoxysilane and glutaraldehyde, and the maximum conductivity was 2.5×10^{-2} $S \cdot cm^{-1}$. All these membranes showed excellent proton conductivities, which were measured under a certain relative humidity. The proton transport in these PVA membranes is due to the mobility of water molecules in the water channel of these membranes. The proton conductivity will decrease significantly at high temperatures, which results in the evaporation of water in the membranes and thus limits proton mobility. The development of membranes, which can be applied at high temperature under anhydrous condition, is demanded [27].

Ionic liquids (ILs) can not only replace water to maintain a channel for proton transfer, but also could donate protons. ILs are receiving much attention owing to their unique properties, such as high thermal stability, high ionic conductivity and environmental friendliness [28]. These advantages of ILs can overcome the restriction of temperatures. In other words, the PEMs with ILs can be used at higher temperatures and meet the demand of environmental protection. Ven et al. [29] prepared a high-temperature proton conductive membrane based on IL of 1-H-3-methylimidazolium bis(trifluoromethanesulfonyl)imide with polybenzimidazole

(PBI). The highest proton conductivity could reach to 1.86 $mS \cdot cm^{-1}$ at 190 ˚C. Eguizábal et al. [30] reported a new kind of high temperature proton exchange membrane, which was composed of the IL of 1-H-3-methylimidazolium bis(trifluoromethanesulfonyl)imide, NH_4BEA, NaY and PBI. The proton conductivity could reach up to 54 $mS \cdot cm^{-1}$ at 200 ˚C. However, the costs of these polymer matrixs are high, so the membrane with low cost and high operating temperature is needed.

In this work, anhydrous proton exchange membranes of PVA have been prepared by the low cost protic ionic liquids (ethylammonium nitrate (EAN), diethylammonium nitrate (DEAN) and triethylammonium nitrate (TEAN)). The controllable structure of the membrane is provided by the PVA support and the proton conductivity can reflect from the protic ionic liquids. The excellent property of novel anhydrous proton exchange membrane is based on the properties of the above materials. The effects of temperature, ILs and crossliker dosage on proton conductivity are also systematically investigated.

2. Experimental

2.1. Materials

PVA (Average M.W. 88,000-97,000 g/mol; 98-99% hydrolyzed). CA (≥ 99.8%) were provided by Alfa Aesar. Nitric acid, ethylamine (≥ 99%), diethylamine (≥ 99%) and triethylamine (≥ 99%) were purchased from Beijing Chemical Reagent Co. All chemicals were used without further purification.

2.2. Preparation of ILs

EAN, DEAN and TEAN (Fig. 1) were synthesized according to the literature [31].

In a typical preparation, 50 ml nitric acid was added to the round bottom flask, 83 ml ethylamine solution was slowly dropped into with vigorous stirring at 0 °C. Then the mixture was purified with a rotary evaporator for removing the water and excess ethylamine. The preparation of DEAN and TEAN were similar to that of EAN.

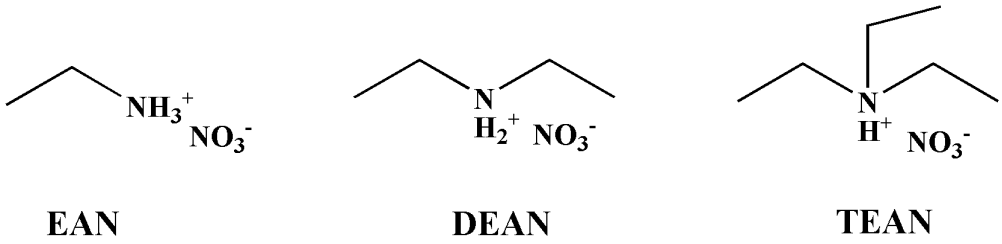

Fig. 1 The chemical structures of ILs.

2.3. Preparation of PVA-CA-IL membranes

PVA (5 g) was dissolved in distilled water (45 ml) at 85 °C. Ionic liquid (EAN, DEAN and TEAN) was added directly into PVA solution with concentrations from 20 to 55 wt%. Then appropriate amount of CA was added into the above mixture solution. The composite membranes were prepared by solution casting method at room temperature. The homogeneous hot solutions were poured into a specific mold [25], and then dried at room temperature. Those composite membranes were peeled off and cross-linked in vacuum drying oven at 120 °C for 2 h. The cross-linked reaction was shown in Fig. 2. After cooling, those crosslinked PVA-IL membranes (PVA-CA-IL) were cut into pieces (ca.1.5×2 cm).

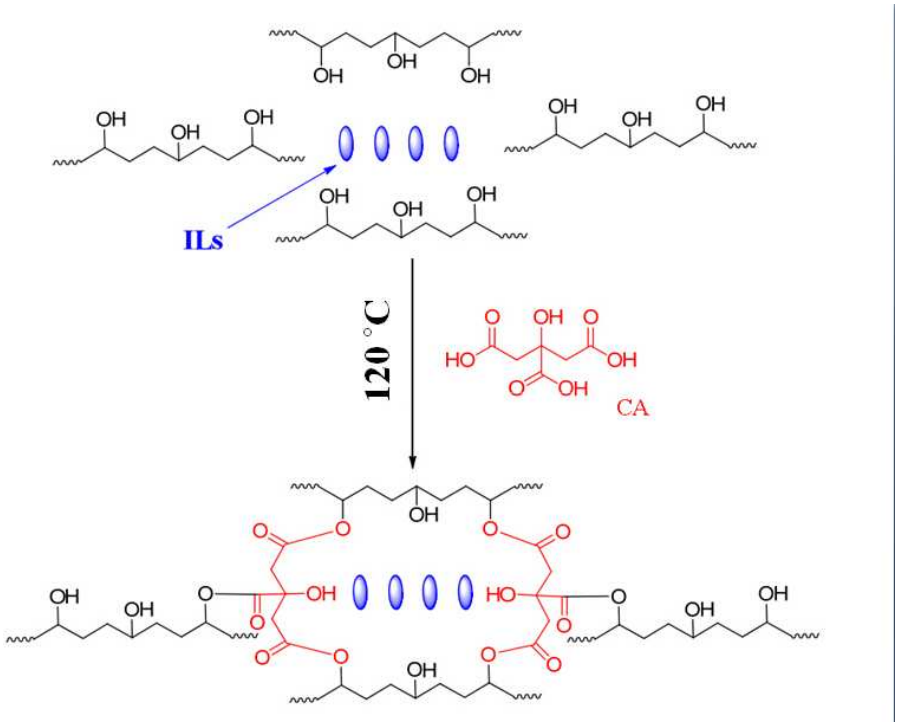

Fig. 2 Possible reaction mechanism of cross-linked PVA-IL membrane. CA served as a crosslinker; IL as proton conductor.

2.4. Structure and Morphology characterization

Fourier transform infrared (FT-IR) spectra were conducted on VERTEX-70 FT-IR spectrometer in the range of 4000 to 500 cm^{-1}. ^{1}H NMR spectroscopy was performed on a Bruker Avance II 300 NMR spectrometer at a resonance frequency of 300 MHz, using D_2O as the solvent and tetramethylsilane (TMS) as an internal standard. The morphologies of composite membranes were characterized using the scanning electron microscope (SEM, JSM-7600F, EOL, Ltd., Japan). The structures of the membranes were investigated using Anton-paar SAX Sess mc2 system (SAXS) with Ni-filtered Cu Kα radiation (0.154 nm) operating at 50 kV and 40 mA. The DSC curves were measured on a Perkin Elmer DSC-8500 instrument at a heating rate of 10 ˚C / min under dry nitrogen.

2.5. Thermal Stability

Thermogravimetric analysis (TGA) was carried out using a Rheometric Scientific TGA1500 (Piscataway, NJ) to investigate the thermal properties of samples. Studies were conducted under inert atmosphere of nitrogen using 8-10 mg samples with a heating rate at 10 ˚C·min^{-1} from ambient temperature to 600 ˚C.

2.6. Proton conductivity

The proton conductivities of the membranes were measured using the electrochemical workstation (660D, CH Instruments, Co., China) with two copper electrodes over the frequency range 1×10^{6} Hz to 1×10^{-4} Hz and placed in the nitrogen atmosphere at anhydrous condition from 40 to 140 ˚C for 2 h before each measurement. The bulk resistance (R_b) was determined from the equivalent circuit analysis by using a frequency response analyzer. The proton conductivity was calculated according to the following equation:

$$\sigma = \frac{\mathrm{L}}{R_b A} \qquad (1)$$

where σ is the proton conductivity, L is the distance between the electrodes, A is the area of the sample [32].

2.7. Mechanical property

Mechanical tensile tests were performed using a Universal Testing Machine (Yashima Works Ltd. Co., model RTM-IT) at room temperature. The crosshead displacement speed of testing was set at the rate of 5 mm·min^{-1}. The membranes with size of 6 mm × 25 mm were used for testing in 35% RH.

Tensile strength (TS) [33] is the stress at the maximum in the plastic portion of the

stress-strain curve that may be sustained by the membrane. Tensile strength was calculated as follows:

$$Ts = F / A_0 \quad (2)$$

Moreover, ductility is another important mechanical property. It is a measure of the degree of plastic deformation that has been sustained at fracture. Ductility (% EL) may be expressed as the percentage of elongation, which was the plastic strain percent at fracture and calculated as follows:

$$\% EL = (l_f - l_0) / l_0 \quad (3)$$

where F is the maximum load, A_0 is the cross section area, l_f and l_0 are the fracture length and original gauge length, respectively.

3. Results and discussion

3.1. Composite membranes characterization

The Fourier transformed infrared attenuated total reflection (FT-IR-ATR) spectra of the membranes were examined by FT-IR, equipped with an ATR accessory, which measured for both top and bottom surfaces. As shown in Fig. 3, all membranes that we prepared exhibit strong absorbance at 1231 and 1718 cm^{-1} which is ascribed to the stretching vibrations of C-O-C and of C=O, respectively. This indicates the occurrence of esterification [34,35]. The stretching vibrations of C-N around 1100 cm^{-1} were also observed in all membranes which illustrates the presence of ILs. Moreover, all membranes show a very strong broad peak around 3300 cm^{-1} for the hydroxyl (O-H) stretching vibration. From these results, it can demonstrate that the PVA-CA-ILs membranes were prepared successfully.

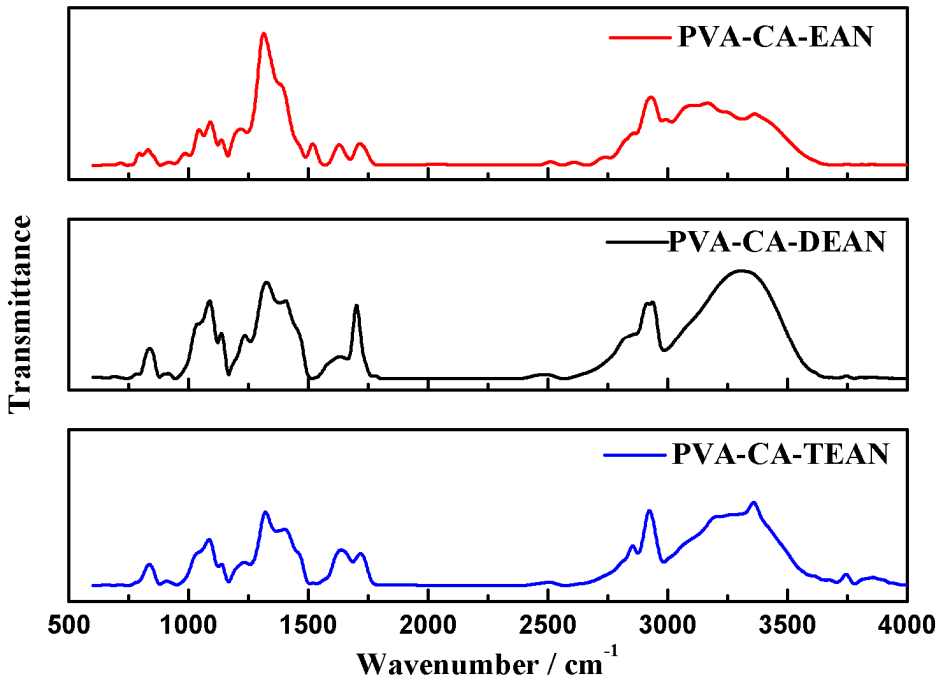

Fig. 3 FT-IR spectra of PVA-CA-IL membranes (molar ratio 1:0.02:0.2).

Fig. 4 shows the TGA curves of PVA-CA (molar ratio 1:0.02), PVA-CA-EAN, PVA-CA-DEAN, and PVA-CA-TEAN (molar ratio 1:0.02:0.2) composite membranes. It is obviously that all membranes exhibit three main weight loss regions, which could be attributed to the thermal salvation, thermal dehydroxylation and deamination, and thermo oxidation [36]. Compared with PVA-CA membrane, the other membranes (PVA-CA-EAN, PVA-CA-DEAN and PVA-CA-TEAN) exhibit an initial weight loss (2-3%) between 50 and 160 ˚C, which is attributed to water desorption indicating the presence of free water loaded by ionic liquids and the strong hydrogen-bond interactions between PVA and ILs [37]. The second weight loss occurs at 160-300 ˚C, which could be attributed to the decomposition of ester bond [38], N-H [39], and NO_3^- [40]. It is obviously that the weight loss of PVA-CA-EAN membrane is more than that of PVA-CA, PVA-CA-DEAN, and PVA-CA-TEAN membranes. It may be due to the

structure of EAN molecular, which possess more N-H groups per molecular than others. Also, the starting decomposition temperatures (160-300 ˚C) of all membranes we prepared are higher than those of traditional PVA membranes which are usually below 80 ˚C [41]. Finally, weight loss at 300-500 ˚C is attributed to the decomposition of PVA backbone [42]. This TGA result illustrates that the composite membranes could be used up to 160 ˚C.

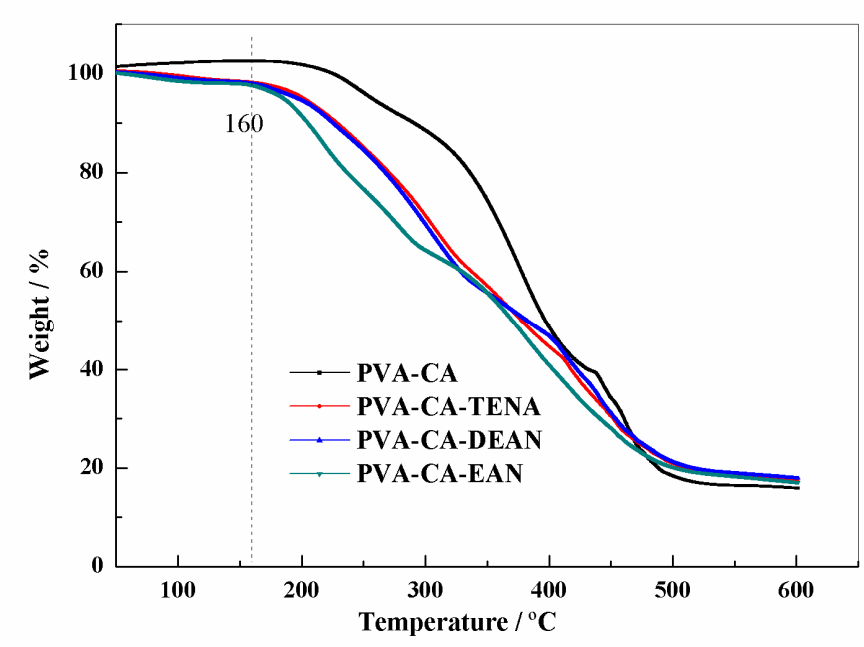

Fig. 4 TGA thermograms of PVA-CA and PVA-CA-IL membranes.

The morphologies of the PVA-CA-EAN membrane's surface and cross-section are shown in Fig. 5. The surface morphology of the composite membranes is smooth, homogeneous and dense (Fig. 5a). The morphologies of membrane surfaces indicate the formation of continuous conducting channels essential for enhancement of proton conductivity [43]. Fig. 5b shows the cross-section image. It is obviously that many little holes are on the cross-section, which could result from the crosslinked reaction at high temperature. Due to the high temperature, the free water could get out of the composite

membranes through these little holes. But the membrane was denser indicating the importance of crosslinked reaction [44].

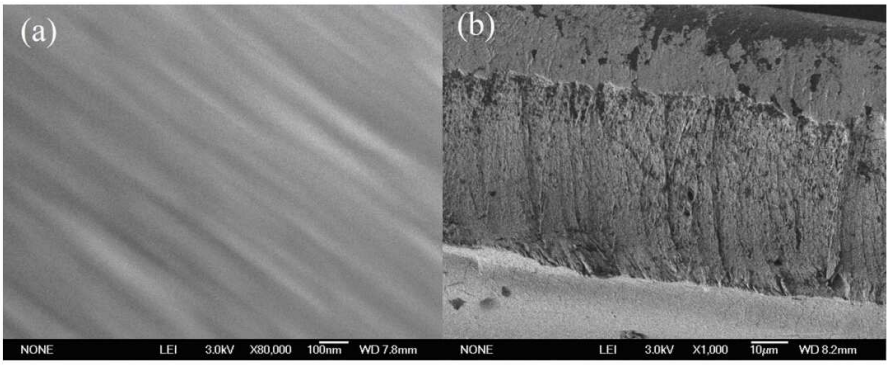

Fig. 5 SEM images of PVA-CA-EAN membrane: (a) surface; (b) cross-section.

In order to further investigate the structure of composite membranes, SAXS was used as the appropriate tool for elucidating the formation of the composite membrane. Fig. 6 shows the SAXS curves of four different composite membranes (PVA-CA, PVA-CA-EAN, PVA-CA-DEAN, and PVA-CA-TEAN). The SAXS curve of PVA-CA membrane displays a 'knee' type curve. It is a single peak and the maximum value of scattering vector q located at 0.18 nm^{-1}, which indicates that PVA-CA membrane is a semi-crystalline structure [45]. For the model of isolated domains embedded in a continuous matrix, the average distance between domains, *d*, can be estimated by the equation below.

$$d=2\pi/q \qquad (4)$$

From this equation, the average distance of the PVA-CA nano-crystallites is 34.9 nm, which is higher than that of pure PVA nano-crystallites (7-20 nm) [46]. This demonstrates that the corss-linked reaction destroyed the hydrogen bonds presented in poly(vinyl alcohol) chain, which is important to stabilize the polymer crystals [47].

When ILs were added into the PVA-CA membranes, the SAXS curves show shoulder peaks. The average values of q increase and the peaks become wide. These results could be due to the intermolecular hydrogen bonds between OH (PVA) and N (Ionic liquids), which shorten the average distance between domains [48]. This shorten distance is benefit for the proton conducting which means that the ionic liquids play a dominant role in the formation of proton exchange membrane. The incorporation of DEAN and TEAN caused the single peaks much broader than that of PVA-CA-EAN membrane, which indicates the better homogeneity of EAN in the PVA structure. The heterogeneous distributions of DEAN and TEAN in the PVA matrix lead to a relatively poor conductivity compared to that of PVA-CA-EAN membrane [48].

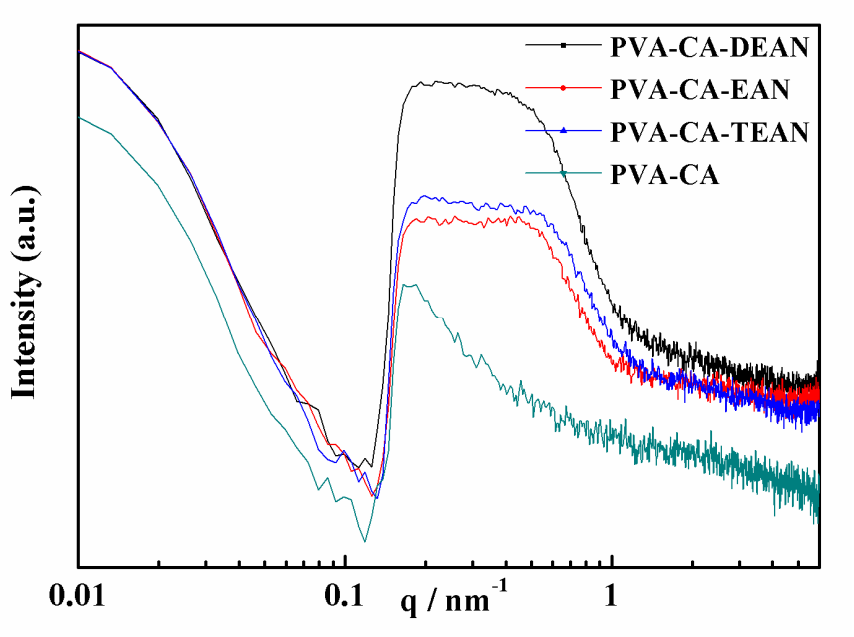

Fig. 6 SAXS spectra of PVA-CA and PVA-CA-IL membranes.

The DSC was used to elucidate the dispersed state of IL in the crosslinked PVA-IL membranes. The PVA-CA-TEAN membrane and pure TEAN were selected to investigate because of the highest melting point of TEAN among the three ionic liquid,

which is easy to observe the change between PVA-CA-TEAN membrane and pure TEAN. In the DSC curve of TEAN, the endothermic peak at ca. 117 ˚C (Fig. 7) is the melting peak of TEAN. However, it is obviously that the melting peak disappeared after inserting TEAN to crosslinked PVA structure. This implies that TEAN embedded inside the membrane is well-dispersed with very small size. The highly dispersed state of TEAN likely results from interactions between TEAN and the polymer matrix. These interactions significantly reduce the size of the IL nanoaggregates [49].

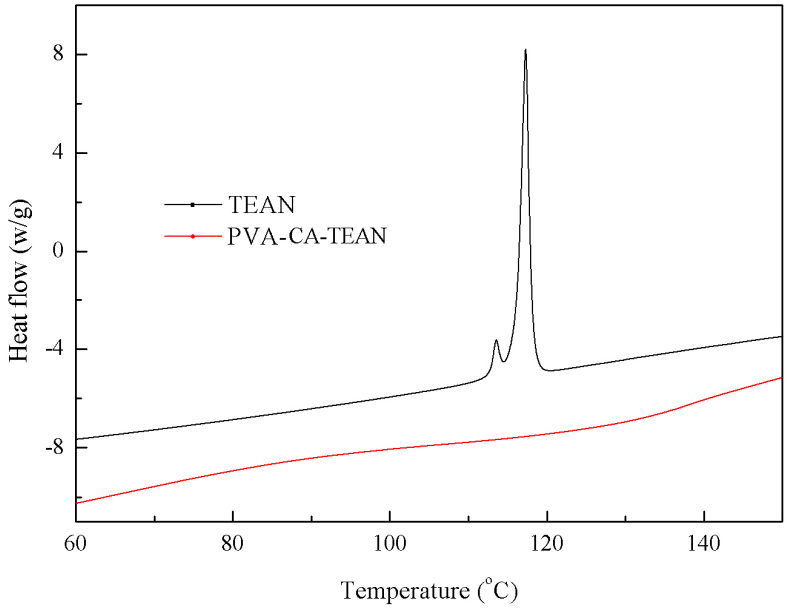

Fig. 7 DSC curves of pure TEAN and PVA-CA-TEAN membrane.

3.2. Proton conductivity of PVA-CA-IL membranes

The proton conductivity is one of the most crucial parameters for characterizing proton conducting membrane [50]. Fig. 8a shows the proton conductivity of the PVA-CA-IL (molar ratio 1:0.02:0.2) composite membranes. The proton conductivities increase sharply with the increase of the tested temperature. The membrane conductivities of PVA-CA-EAN, PVA-CA-DEAN, and PVA-CA-TEAN membranes

could reach to 1.1, 1.5, and 0.4 mS·cm^{-1} at 140 °C, respectively. It is obviously that the conductivity of PVA-CA-DEAN is higher than that of PVA-CA-EAN though the distributions of the DEAN is poor than that of EAN. This may be attributed higher iconicity of DEAN which is benefit to the proton conductivity [51]. The proton vonductivity of PVA-CA-TEAN is lowest among the three PVA-CA-IL composite membranes. This is attributed to the great steric hindrance, which hinders the proton transfer [3].

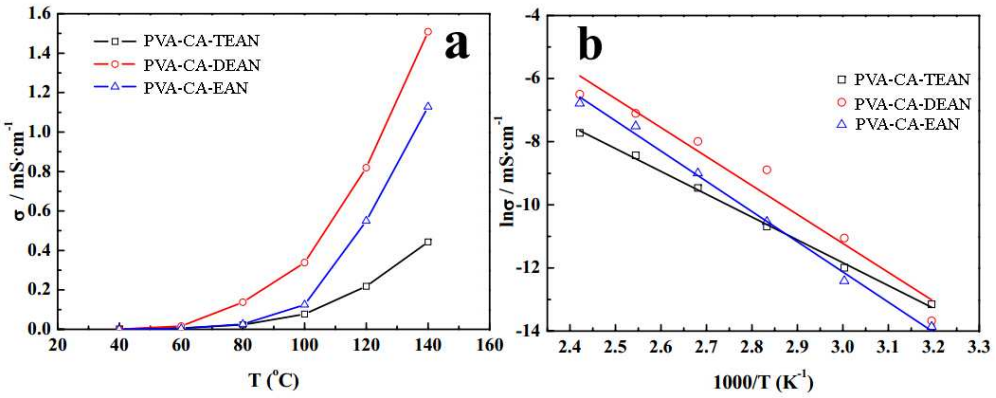

Fig. 8 (a) The proton conductivities of PVA-CA-IL membranes as a function of temperatures (molar ratio PVA:CA:IL=1:0.02:0.2) and (b) temperature dependence of proton conductivity.

The apparent activation energy (E_a) for PVA-CA-IL composite membranes was estimated using the following equation [52]:

$$\ln \sigma = -\frac{E_a}{RT} \qquad (5)$$

Where σ is the proton conductivity, R is the universal gas constant, and T is the absolute temperature.

As shown in Fig. 8b, the changing trend of lnσ depends almost linearly on 1/T. The E_a values of three PVA-CA-IL membranes are shown in Table 1. All the E_a values

are higher than that of Nafion 117 [53]. This indicates that the proton mobility in PVA-CA-IL composite membrane is limited, which could attribute to the bulky size of the IL [54].

Table 1

Ea values of PVA-CA-IL membranes and Nafion 117.

Composite membrane	Slope	Activation energy ($kJ \cdot mol^{-1}$)
PVA-CA-TEAN	-7.24	60
PVA-CA-DEAN	-9.17	76
PVA-CA-EAN	-9.58	80
Nafion 117	--	13

3.3. Effect of IL dose

In order to investigate the effect of IL dosage on the proton conductivity, we measured the conductivities of PVA-CA-EAN (molar ratio PVA:CA=1:0.1) membranes with different dosage of IL at 100 ˚C. As shown in Fig. 9, with the increase of IL dosage, proton conductivity increases sharply when the mass percent of IL is higher than 42.4%. This may be due to the higher proton density (the proton number per unit volume) which can lead to an increase of proton conductivity of PVA-CA-IL composite membrane [55]. The maximum conductivity is 6.5 $mS \cdot cm^{-1}$ at 100 ˚C, which is higher than that of diethylethylammonium trifluoromethanesulfonate (IL) doped hybrid membrane (5.4 $mS \cdot cm^{-1}$) at 100 ˚C [56], 1-butyl-3-methyl imidazolium bis(trifluoromethanesulfonyl)imide doped sulfonated poly (ether ketone) membrane (1.3 $mS \cdot cm^{-1}$) [57] at 100 ˚C and H_3PO_4 doped PVA/PAM membrane (5.25 $mS \cdot cm^{-1}$) at

180 ˚C [58].

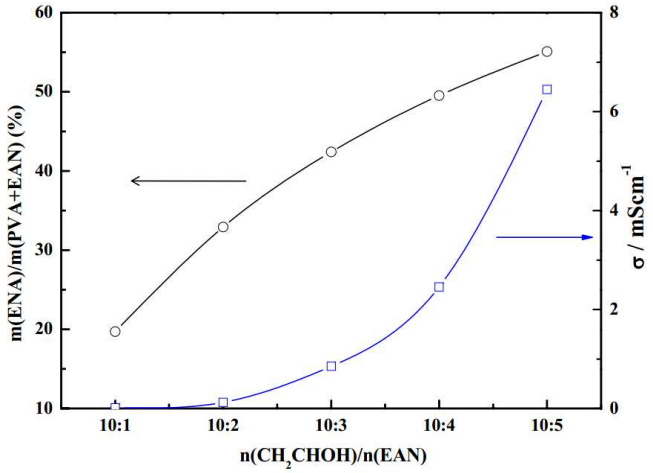

Fig. 9 The effect of IL dosage on proton conductivity of PVA-CA-EAN membrane measured at 100 ˚C.

3.4. Effect of CA dose

The crosslinker (CA) played an important role in the preparation of PVA-IL composite membrane. Firstly, the crosslinker can make the membrane more compact and rigid which is beneficial to the Young's modulus, tensile strength and oxidative stability of membrane [59,60]. Secondly, notably, the crosslinking degree of polymer could affect the proton conductivity of PVA-IL composite membrane. Therefore, it is important to investigate CA dosage in PVA-IL (molar ratio PVA:EAN=1:0.4) composite membranes. When the mole ratio of CA / PVA was 0.1:1, with temperature increase, the increase of the proton conductivity become relatively slow (Fig. 9a). This indicates that the mobility of the proton is limited in the high crosslinked composite membrane. In other words, the high crosslinking degree hinders the proton mobility [61]. The mole ratio of CA / PVA was changed to 0.05:1. With increasing temperature, the curve shows a sharply increase (Fig. 10a). The maximum conductivity can reach to

7.8 mS·cm^{-1} at 140 °C. This implies that the lower crosslinking degree is beneficial to the proton conductivity. However, it's noted that the tensile strength decreased when decreasing the mole ratio of CA / PVA (Table 2). When the crosslinking degree is low enough, the structures of membrane maybe can't maintain a fixed shape at high temperature with poor mechanical property. So it is important to choose the CA dosage for balancing the proton conductivity and poor mechanical property of the membranes.

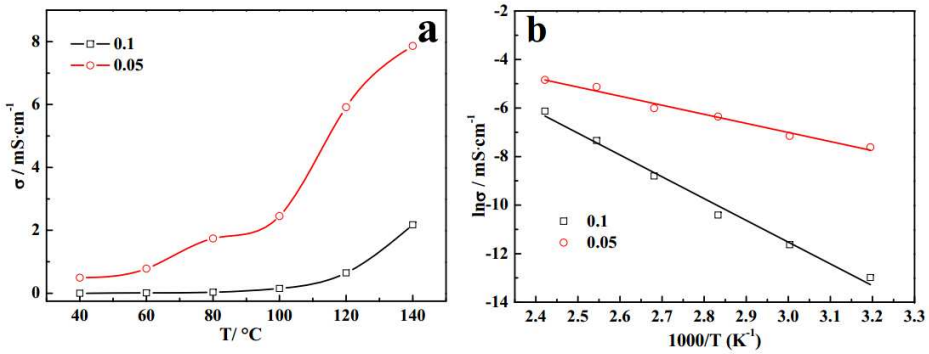

Fig. 10 (a) The effect of CA dosage on proton conductivity of PVA-CA-EAN membrane measured at different temperatures and (b) temperature dependence of proton conductivity (lnσ-1000/T).

Fig. 10b shows a linear relationship between lnσ and 1/T. The calculated values are shown in Table 2. Comparing the membrane with different CA dosages, the E_a of PVA-CA-EAN (mole ratio=1:0.05:0.4) is lower. The lowest Ea value of proton conductivity indicates the least energy needed for proton transfer in the membranes [62]. Fixing the CA dosage, the dosage of EAN was reduced by half. The result shows that the E_a of PVA-CA-EAN (mole ratio=1:0.05:0.4) reaches up to 80 kJ·mol^{-1} (Table 2). All this results indicate the importance of CA and EAN dose on elevating the proton conductivity.

Table 2

Ea values and mechanical stability of PVA-CA-EAN membranes with different molar ratios and Nafion 117.

Composite membrane	Slope	Activation energy ($kJ \cdot mol^{-1}$)	Tensile strength (MPa)	Elongation (%)
PVA-CA-EAN(1:0.1:0.4)	-8.97	75	10.7	320.4
PVA-CA-EAN(1:0.05:0.4)	-3.73	31	8.8	314.7
PVA-CA-EAN(1:0.05:0.2)	-9.58	80	--	--
Nafion 117	--	13	14.2	--

4. Conclusion

A series of novel anhydrous proton exchange membranes (PVA-CA-IL) were prepared using the low cost ionic liquids of EAN, DEAN, TEAN, and the polymer of PVA. All the composite membranes PVA-CA-IL could be applied at high temperatures, and also had smooth morphologies of surfaces, which can establish the continuous conducting channels to enhance the proton conductivity. IL played an important role in PVA-CA-IL anhydrous proton exchange membrane and did not present alone in the composite structure. The IL and crosslinker dosage had an important effect on proton conductivity. The maximum conductivity was 7.8 $mS \cdot cm^{-1}$ at 140 ˚C, which was higher than reported values. This work may provide a new approach for the research and development of new anhydrous proton exchange membrane.

Acknowledgments

The authors are grateful to the National Basic Research Program (2013CB834505),

Specialized Research Fund for the Doctoral Program of Higher Education of China (No.20120131130003) and the Shandong Provincial Natural Science Foundation, China (ZR2012BZ001).

References

1 E. A. Mistri and S. Banerjee, *RSC Adv.*, 2014, **4**, 22398-22410.

2 C. M. Chang, H. Y. Li, J. Y. Laia and Y. L. Liu, *RSC Adv.*, 2013, **3**, 12895-12904.

3 H. Cheng, J. Xu, L. Ma, L. Xu, B. Liu, Z. Wang and H. Zhang, *J. Power Sources*, 2014, **260**, 307-316.

4 Y. Zhang, X. Fei, G. Zhang, H. Li, K. Shao, J. Zhu, C. Zhao, Z. Liu, M. Han and H. Na, *Int. J. Hydrogen Energy*, 2010, **35**, 6409-6417.

5 S. Zhou and D. Kim, *Electrochim. Acta*, 2012, **63**, 238-244.

6 M. A. Hickner, H. Ghassemi, Y. S. Kim, B. R. Einsla and J. E. McGrath, *Chem. Rev.*, 2004, **104**, 4587-4612.

7 J. A. Kerres, *J. Membr. Sci.*, 2001, **185**, 3-27.

8 Y. Di, W. Yang, X. Li, Z. Zhao, M. Wanga and J. Dai, *RSC Adv.*, 2014, **4**, 52001-52007.

9 B. Wang, Z. Cai, N. Zhang, B. Zhang, D. Qi, C. Zhao and H. Na, *RSC Adv.*, 2015, **5**, 536-544.

10 C. Ke, J. Li, X. Li, Z. Shao and B. Yi, *RSC Adv.*, 2012, **2**, 8953-8956.

11 G. Jiang, J. Qiao and F. Hong, *Int. J. Hydrogen Energy*, 2012, **37**, 9182-9192.

12 Q. Tang, G. Qian and K. Huang, *RSC Adv.*, 2013, **3**, 3520-3525.

13 S. J. Peighambardoust, S. Rowshanzamir and M. Amjadi, *Int. J. Hydrogen Energy*, 2010, **35**, 9349-9384.

14 C. Schmidt, T. Glück and G. Schmidt-Naake, *Chem. Eng. Technol.*, 2008, **31**, 13-22.

15 J. Prabhuram, T. S. Zhao, Z. X. Liang, H. Yang and C.W. Wong, *J. Electrochem. Soc.*,

2005, **152**, A1390-A1397.

16 O. Savadogo, *J. Power Sources*, 2004, **127**, 135-161.

17 D. Guptaa, A. Madhukarb and V. Choudhary, *Int. J. Hydrogen Energy*, 2013, **38**, 12817-12829.

18 Z. Yao, Z. Zhang, L. Wu and T. Xu, *J. Membr. Sci.*, 2014, **455**, 1-6.

19 P. H. Su, J. Cheng, J. F. Li, Y. H. Liao and T. L. Yu, *J. Power Sources*, 2014, **260**, 131-139.

20 V. V. Binsu, R. K. Nagarale and V. K. Shahi, *J. Mater. Chem.*, 2005, **15**, 4823-4831.

21 J. Won, H. H. Park, Y. J. Kim, S. W. Choi, H. Y. Ha, I. H. Oh, H. S. Kim, Y. S. Kang and K. J. Ihn, *Macromolecules*, 2003, **36**, 3228-3234.

22 D. S. Kim, H. B. Park, J.W. Rhim and Y. M. Lee, *J. Membr. Sci.*, 2004, **240**, 37-48.

23 K. D. Kreuer, *J. Membr. Sci.*, 2001, **185**, 29-39.

24 D. S. Kim, I. C. Park, H. I. Cho, D. H. Kim, G. Y. Moon, H. K. Lee and J. W. Rhim, *J. Ind. Eng. Chem.*, 2009, **15**, 265-269.

25 A. D. Gomes and J. C. Dutra, *Int. J. Hydrogen Energy*, 2012, **37**, 6246-6252.

26 U. Thanganathan and M. Nogami, *J. Solid State Electrochem.*, 2014, **18**, 97-104.

27 Q. Tang, G. Qian and K. Huang, *RSC Adv.*, 2012, **2**, 10238-10244.

28 H. Gao, T. Kan, S. Zhao, Y. Qian, X. Cheng, W. Wu, X. Wang and L. Zheng, *J. Hazard. Mater.*, 2013, **261**, 83-90.

29 E. V. D. Ven, A. Chairuna, G. Merle, S. P. Benito, Z. Borneman and K. Nijmeijer, *J. Power Sources*, 2013, **222**, 202-209.

30 A. Eguizábal, J. Lemus and M. P. Pina, *J. Power Sources*, 2013, **222**,483-492.

31 D. F. Evans, S. H. Chen, G. W. Schriver and E. M. Arnett, *J. Am. Chem. Soc.*, 1981, **103**, 481-482.

32 C. S. Wu, F. Y. Lin, C. Y. Chen and P. P. Chu, *J. Power Sources*, 2006, **160**, 1204-1210.

33 C. P. Liu, C. A. Dai, C. Y. Chao and S. J. Chang, *J. Power Sources*, 2014, **249**, 285-298.

34 J. Gao, J. X. Lei and X. G. Lei, *Acta Polymerica Sinica*, 2001, **1**, 118-120.

35 Y. Yang, H. Gao, F. Lu and L. Zheng, *Int. J. Hydrogen Energy*, 2014, **39**, 17191-17200.

36 C. A. Dai, C. P. Liu, Y. H. Lee, C. J. Chang, C. Y. Chao and Y.Y. Cheng, *J. Power Sources*, 2008, **177**, 262-272.

37 J. S. Yang, Q. T. Che, L. Zhou, R. H. He and R. F. Savinell, *Electrochim. Acta*, 2011, **56**, 5940-5946.

38 M. S. Boroglu, S. U. Celik, A. Bozkurt and I. Boz, *J. Membr. Sci.*, 2011, **375**, 157-164.

39 S. Luoa, X. Xua, G. Zhoua, C. Liua, Y. Tangb, Y. Liu, *J. Hazard. Mater.*, 2014, **274**, 145-155.

40 F. Cataldoa, O. Ursinic, C. Cherubinic, S. Rocchic, *Polym. Degrad. Stabil.*, 2012, **97**, 1090-1100.

41 L. Zhang, S. R. Chae, Z. Hendren, J. S. Park and M.R. Wiesner, *Chem. Eng. J.*, 2012, **204-206**, 87-97.

42 C. E. Tsai, C. W. Lin and B. J. Hwang, *J. Power Sources*, 2010, **195**, 2166-2173.

43 Y. Zhang, J. W. Y. Ting, R. Rohan, W. Cai, J. Li, G. Xu, Z. Chen, A. Lin and H. Cheng, *J. Mater. Sci.*, 2014, **49**, 3442-3450.

44 L. Lebrun, E. Da Silva and M. Metayer, *J. Appl. Polym. Sci.*, 2002, **84**, 1572-1580.

45 H. S. Mansur, C. M. Sadahira, A. N. Souza and A. A. P. Mansur, *Mat. Sci. Eng. C*, 2008, **28**, 539-548.

46 H. S. Mansur, R. L. Oréfice and A. A. P. Mansur, *Polymer*, 2004, **45**, 7193-7202.

47 R. M. Hodge, G. H. Edward and G. P. Simon, *Polymer*, 1996, **37**, 1371-1376.

48 F. Lu, X. Gao, X. Yan, H. Gao, L. Shi, H. Jia and L. Zheng, *ACS Appl. Mater. Interfaces*, 2013, **5**, 7626-7632.

49 V. D. Noto, M. Piga, G. A. Giffin, S. Lavina, E. S. Smotkin, J. Y. Sanchez and C. Iojoiu, *J. Phys. Chem. C*, 2012, **116**, 1361-1369.

50 Y. W. Zhang, Z. G. Zhang, W. Chen, C. P. Liu, W. Xing and S.B. Zhang, *J. Power Sources*, 2014, **258**, 5-8.

51 T. L. Greaves, A. Weerawardena, I. Krodkiewska and C. J. Drummond, *J. Phys. Chem. B*, 2008, **112**, 896-905.

52 B. Lin, S. Cheng, L. Qiu, F. Yan, S. Shang, J. Lu, *Chem. Mater.*, 2010, **22**, 1807-1813.

53 B. Lin, L. Qiu, J. Lu and F. Yan, *Chem. Mater.*, 2010, **22**, 6718-6725.

54 T. Zhou, J. Zhang, J. Qiao, L. Liu, G. Jiang, J. Zhang and Y. Liu, *J. Power Sources*, 2013, **227**, 291-299.

55 J. E. Kim and D. Kim, *J. Membr. Sci.*, 2012, **405-406**, 76-184.

56 W. H. Luo and L. H. Zhao, *J. Membr. Sci.*, 2014, **451**, 32-39.

57 R. S. Malik, S. N. Tripathi, D. Gupta and V. Choudhary, *Int. J. Hydrogen Energy*, 2014, **39**, 12826-12834.

58 Q. Tang, K. Huang, G. Qian and B.C. Benicewicz, *J. Power Sources*, 2013, **229**, 36-41.

59 C. H. Shen and S. L. Hsu. *J. Membr. Sci.*, 2013, **443**, 138-143.

60 J. Wang, J. Wang and S. Zhang, *J. Membr. Sci.*, 2012, **415-416**, 205-212.

61 J. Zhua, G. Zhanga, K. Shaob, C. Zhaoa, H. Lia, Y. Zhanga, M. Hana, H. Lina, M. Lia and H. Na, *J. Power Sources*, 2011, **196**, 5803-5810.

62 B. C. Lin, L. H. Qiu, J. M. Lu, F. Yan, *Chem. Mater.*, 2010, **22**, 6718-6725.

Figure captions:

Fig. 1 The chemical structures of ILs.

Fig. 2 Possible reaction mechanism of cross-linked PVA-IL membrane. CA served as a crosslinker; IL as proton conductor.

Fig. 3 FT-IR spectra of PVA-CA-IL membranes (molar ratio 1:0.02:0.2).

Fig. 4 TGA thermograms of PVA-CA and PVA-CA-IL membranes.

Fig. 5 SEM images of PVA-CA-EAN membrane: (a) surface; (b) cross-section.

Fig. 6 SAXS spectra of PVA-CA and PVA-CA-IL membranes.

Fig. 7 DSC curves of pure TEAN and PVA-CA-TEAN membrane.

Fig. 8 (a) The proton conductivities of PVA-CA-IL membranes as a function of temperatures (molar ratio PVA:CA:IL=1:0.02:0.2) and (b) temperature dependence of proton conductivity.

Fig. 9 The effect of IL dosage on proton conductivity of PVA-CA-EAN membrane measured at 100 ˚C.

Fig. 10 (a) The effect of CA dosage on proton conductivity of PVA-CA-EAN membrane measured at different temperatures and (b) temperature dependence of proton conductivity (lnσ-1000/T).

Table captions

Table 1 Ea values of PVA-CA-IL membranes and Nafion 117

Table 2 Ea values and mechanical stability of PVA-CA-EAN membranes with different molar ratios and Nafion 117.